Research Article Vol. 40, No. 9 / September 2023 / Journal of the Optical Society of America B 2429

Journal of the Optical Society of America B

OPTICAL PHYSICS

Generation of 107 W, 1.07 mJ femtosecond pulses from chirped- and divided-pulse Sagnac Yb-fiber amplifiers by suppression of static mode degradation

Zhuo Shi,[1,2] Jingshang Wang,[1,2] Yao Zhang,[1,3] Junli Wang,[3] Zhiyi Wei,[1,2,4] and Guoqing Chang[1,2,4,*]

[1]Beijing National Laboratory for Condensed Matter Physics, Institute of Physics, Chinese Academy of Sciences, Beijing 100190, China
[2]University of Chinese Academy of Sciences, Beijing 100049, China
[3]School of Physics and Optoelectronic Engineering, Xidian University, Xi'an 710071, China
[4]Songshan Lake Materials Laboratory, Dongguan, Guangdong 523808, China
*guoqing.chang@iphy.ac.cn

Received 30 June 2023; revised 6 August 2023; accepted 9 August 2023; posted 9 August 2023; published 22 August 2023

We investigate the effect of static mode degradation (SMD) on the power scaling of mJ-level Sagnac Yb-fiber amplifiers. We find that SMD can be effectively suppressed by inserting a polarization-filtering device between two rod-type fibers. Consequently, the resulting amplifier system exhibits improved combining efficiency and average power, and it can deliver 240 fs pulses with 1.07 mJ energy and 107 W average power. This mJ femtosecond source of hundred-watt average power is of particular importance for high-field science applications.

https://doi.org/10.1364/JOSAB.499313

1. INTRODUCTION

Yb-doped ultrafast fiber laser systems based on chirped-pulse amplification (CPA) have achieved rapid progress in recent years. Thanks to the development of double-clad Yb-fibers with large mode area, a single-channel Yb-fiber CPA system can generate femtosecond pulses with pulse energy up to 2.2 mJ [1] or average power up to 1 kW [2]. Further scaling the average power and pulse energy spurred the development of two techniques—coherent beam combining (CBC) and divided pulse amplification (DPA), which involves spatially and temporally splitting pulses and recombining them after amplification. For example, Stark *et al.* combined 16 channels with 128 pulse replicas to achieve pulse energy up to 32 mJ [3]; Müller *et al.* employed coherent combination of 12 fiber amplifiers to obtain femtosecond pulses with the average power up to 10.4 kW [4]. It is essential for CBC and DPA to maintain the coherence of pulse replicas, which usually involves a complex and expensive electronic feedback system to actively control the phase of all replicas.

On the other hand, generation of mJ-level femtosecond pulses with hundred-watt-level average power can be achieved via passively stabilized pulse combination. By proper design of the amplification architecture, both CBC and DPA can be realized without active electronic control elements [5]. Among several feasible configurations, passive CBC based on Sagnac interferometers is attractive because the two counterpropagating beams exhibit excellent resistance to thermal and mechanical disturbance and, thus, maintain high combining efficiency at large accumulated nonlinearities [6]. In 2012, Zaouter *et al.* employed such a Sagnac interferometer to combine two rod-type Yb-fiber chirped-pulse amplifiers; the resulting system delivered 650 μJ at 96 kHz with an average power of 60 W [7]. To further increase the pulse energy, Daniault *et al.* introduced DPA into the Sagnac interferometer [8]; that is, the pulse was temporally divided before the spatial split in the Sagnac interferometer [9–12].

Figure 1(a) illustrates a typical Sagnac amplifier based on Yb-fibers, in which the two fiber amplifiers are identical and arranged with mirror symmetry. In this scenario, the operation of each channel is equivalent to an amplifier configured in double-pass, as schematically shown in Fig. 1(b). Recently, Lupi *et al.* demonstrated up to 120 W average power in a double-pass amplifier, and further power scaling is limited by static mode degradation (SMD) [13]. SMD arises from coupling between fundamental mode and higher-order modes through the thermo-optic nonlinear grating induced by two counterpropagating optical beams inside the fiber amplifier. The counterpropagating modes have the same frequency, and the induced thermo-optic grating is static [14]. This is in contrast with transverse mode instability (TMI) [15–18], in which the thermo-optic grating is caused by two co-propagating beams

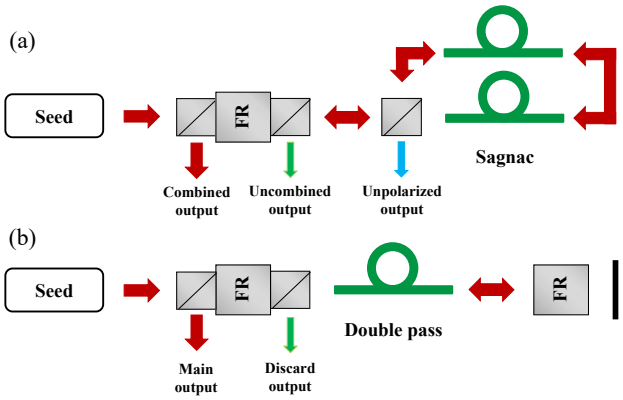

Fig. 1. Schematic comparison between (a) Sagnac fiber amplifier and (b) double-pass fiber amplifier.

that render a moving grating light and, thus, a dynamic power exchange between the fundamental mode and higher-order modes [19]. SMD in double-pass fiber amplifiers has been explored and analyzed by several studies [12,20–22]. It has been found that polarization plays an important role in the double-pass configuration, as polarization rotation is needed to separate input and output beam by polarizing beam splitter (PBS). We observed unexpected nonlinear polarization rotation effect associated with SMD, which caused additional energy transfer from the main output to the discard output [20]. Fortunately, inserting a polarizer filter between the first and second passes in double-pass configuration can effectively suppress the SMD effect [21].

Given that each fiber amplifier in a Sagnac loop may be treated as a double-pass fiber amplifier, one may ask: what is the effect of SMD on power scaling of a Sagnac fiber amplifier? In the previous implementations of Sagnac fiber amplifiers, polarizing devices (such as the PBS) are absent between the two rod-type fiber amplifiers [23]. In this paper, we explore how the SMD affects the power scalability of Sagnac interferometer and combining efficiency. By introducing a polarization-filtering device to mitigate SMD, our Sagnac Yb-fiber amplifier system can generate 1.07 mJ, 240 fs pulses with 107 W average power.

2. EXPERIMENTAL SETUP

Figure 2 shows the experimental setup. Consisting of a passively mode-locked Yb-fiber oscillator, a stretcher, a pulse picker, and two fiber preamplifiers, the all-fiber front end delivers a stretched pulse centered at 1033 nm with a duration of 600 ps. The pulse energy is 0.8 μJ, and the repetition rate can be adjusted from 100 kHz to 1 MHz by a pulse picker. An optical isolator including by two PBSs (PBS1 and PBS2), a Faraday rotator (FR1), and a half-wave plate (HWP1) is placed after the front end. Two PBSs (PBS3 and PBS4) and two mirrors form an unbalanced Mach–Zehnder interferometer, and the path length difference between the two arms creates two orthogonally polarized replicas temporarily separated by 1.8 ns. Adjusting the angle of HWP2 changes the energy fraction distributed in each replica. The following FR2 and HWP3 control the spatial division ratio of forward pulses and rotate the polarization of backward pulses.

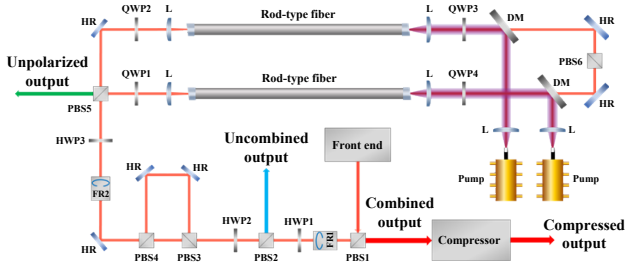

Fig. 2. Experimental setup of the passively combined divided-pulse and Sagnac-type amplifier. PBS, polarizing beam splitter; FR, Faraday rotator; HWP, half-wave plate; QWP, quarter-wave plate; HR, high-reflection mirror; and DM, dichroic mirror.

Each temporal pulse replica is split by PBS5 into two beams that propagate clockwise (CW) and counterclockwise (CCW) through a Sagnac interferometer including two symmetrically arranged rod-type Yb-doped fibers. Each fiber (NKT, aeroGAIN-ROD-PM85) is 0.8 m long with a core diameter of 85 μm. They each are pumped by a laser diode centered at 976 nm with a full power of 500 W. Two quarter-wave plates (i.e., QWP1 and QWP2) convert the input-beam polarization from linear to circular in order to reduce accumulated nonlinearities [24]. After the first amplification, both CW and CCW beams become slightly elliptically polarized due to SMD. Without correcting the polarization, stronger SMD during the second amplification increases the polarization ellipticity of two beams. As a result, an increased portion of recombined power is directed to the exit port labeled as unpolarized output (green arrow in Fig. 2). In this submission, we introduce another two QWPs (i.e., QWP3 and QWP4) and a PBS (i.e., PBS6) between two rod-type fibers. They constitute a polarization-filtering device that restores circular polarization to the optical beam prior to the second amplification and, therefore, effectively suppress SMD-caused polarization degradation. After traveling a circle through the Sagnac interferometer, the CW and CCW beams are coherently combined and propagate back to HWP3. At this point, the four spatiotemporal pulse replicas are recombined into two temporal replicas, which return to the Mach–Zehnder interferometer and are passively recombined at PBS3. The part of all four spatiotemporal pulse replicas with different phase, spectrum, or spatial distribution is removed at PBS2 as the uncombined output, while the major part becomes the combined output at PBS1. Finally, the combined pulses are sent to a double-pass diffraction grating compressor including two 1740 l/mm gratings.

3. EXPERIMENTAL RESULTS

A. Effect of Polarization Filter on Power Scaling

To explore the average power limitation of Sagnac fiber amplifiers delivering mJ-level pulse energy, we operated the system at a repetition rate of 150 kHz. The results in Figs. 3(a) and 3(b) illustrate the effect of the polarization-filtering device on the performance of our Sagnac fiber amplifier. In the figures, the red diamonds, blue squares, and black circles represent the average powers at the ports of combined output, uncombined output, and unpolarized output, respectively. The total power denoted as purple triangles corresponds to the power summation of all

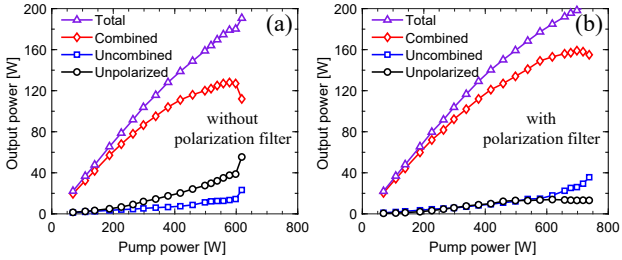

Fig. 3. Total power (purple triangles), combined power (red diamonds), uncombined power (blue squares), and unpolarized power (black circles) as a function of total pump power for two cases: (a) without the polarization filter and (b) with the polarization filter.

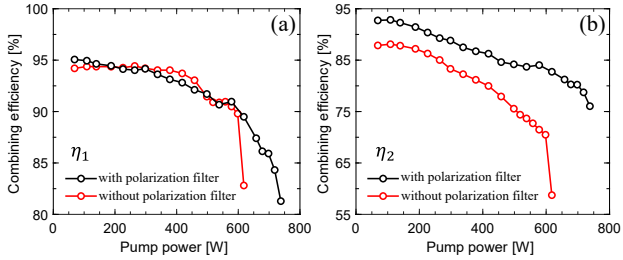

Fig. 4. (a) η_1 and (b) η_2 as a function of total pump power with (black) and without (red) polarization filter inside the amplifier system for 150 kHz repetition rate.

the three outputs. Figure 3(a) shows the dependence of total power, combined power, uncombined, and unpolarized power on the total pump power as PBS6 was removed. As the pump power increases, the growth of the combined power gradually slows down while the uncombined power and the unpolarized power both undergo accelerated increase. At 600 W pump power, the combined power reaches a maximum value of 128 W, and the average powers at the uncombined output and the unpolarized output are 14 W and 38 W, respectively. Further increasing the pump power causes continuous-wave lasing at 1033 nm, manifesting as an abrupt drop of the combined power and an increase of the uncombined power and the unpolarized power.

Figure 3(b) illustrates the results with the polarization filter added into the system. While the total power and uncombined power have negligible change, the unpolarized power is substantially suppressed to the level of uncombined output at low pump power and reaches saturation at a pump power of 500 W. Thanks to the mitigation of SMD, the power saved from the unpolarized output mainly transfers to the combined output. The new maximum of combined average power is 160 W at a pump power of 700 W. For the pump power increasing from 700 W to 740 W of pump power, the combined output slightly decreases to 155 W, while the uncombined output increases from 26 W to 36 W. We believe the power exchange between the combined and uncombined output is mainly due to SMD-induced profile change of counterpropagation beams [14].

Combining efficiency is an important parameter to quantify the performance of a coherent combination system. As for Sagnac amplifier, Guichard *et al.* proposed the following definition of combining efficiency [23]:

$$\eta_1 = \frac{P_{\text{combined}}}{P_{\text{combined}} + P_{\text{uncombined}}}, \tag{1}$$

where P_{combined} and $P_{\text{uncombined}}$ represent combined and uncombined output powers, respectively. Apparently, the unpolarized power is excluded from measuring the combining efficiency. Indeed, the unpolarized power is associated with the performance of spatial combination, and we propose to include it in the definition of the combining efficiency:

$$\eta_2 = \frac{P_{\text{combined}}}{P_{\text{combined}} + P_{\text{uncombined}} + P_{\text{unpolarized}}}, \tag{2}$$

where $P_{\text{unpolarized}}$ represents the output power at the unpolarized output port.

To show the difference between these two definitions, Figs. 4(a) and 4(b) plot η_1 and η_2 as a function of pump power, respectively. In each figure, the black (red) curve shows the results corresponding the polarization filter being removed (added). As Fig. 4(a) shows, the combining efficiency η_1 changes little under the two situations, both of which decrease from 95% at a pump power of 70 W to 90% at a pump power of 600 W. In contrast, the results in Fig. 4(b) show that the combining efficiency of the new definition η_2 becomes much more sensitive to the presence or absence of the polarization-filtering device. With the polarization filter included in the system, η_2 decreases from 93% to 83% as the pump power increases from 70 W to 600 W [black curve in Fig. 4(b)]. Without the polarization filter, η_2 drops from 88% to 70% in the same range of pump power variation [red curve in Fig. 4(b)].

B. Generation of Millijoule Pulses at 100 kHz Repetition Rate

To generate mJ-level pulses with stable power and high beam quality from the Sagnac amplifier, we operate the setup at a lower repetition rate of 100 kHz with the polarization filtering device incorporated into the system. As Fig. 5(a) shows, the combined and uncombined outputs increase linearly with the pump power and reach 117 W and 10 W at a pump power of 420 W, respectively. The increase of the unpolarized power slows down at 7.5 W when the pump power exceeds 340 W indicating suppression of the SMD-induced depolarization effect. The combining efficiency η_2 is shown in Fig. 5(b), which changes from 92% to 87% as the pump power increases from 70 W to 420 W. The decrease of combining efficiency is mainly due to phase mismatch among four spatiotemporal replicas caused by nonlinearities [25,26]. When working at high gain level, the gain of spatiotemporal pulse replicas decreases with time, which introduces different nonlinear phase shifts to all four spatiotemporal pulse replicas through self-phase modulation and Kramers–Krönig coupling. The phase mismatch can be partly compensated by adjusting the proportion of energy distributed to each spatiotemporal replica, which is realized by changing the angle of HWP2 and HWP3. The residual phase mismatch is detrimental to the combination of pulse replicas.

The combined output before compression reaches 117 W at the maximum pump power of 420 W. These amplified pulses

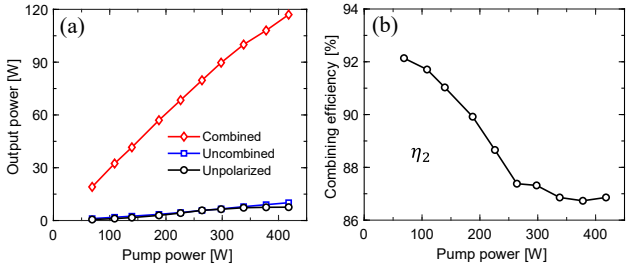

Fig. 5. (a) Average power at different outputs and (b) combining efficiency versus total pump power with polarization filter inside the amplifier system for 100 kHz repetition rates. Red diamonds, blue squares, and black circles represent combined, uncombined, and unpolarized output power, respectively.

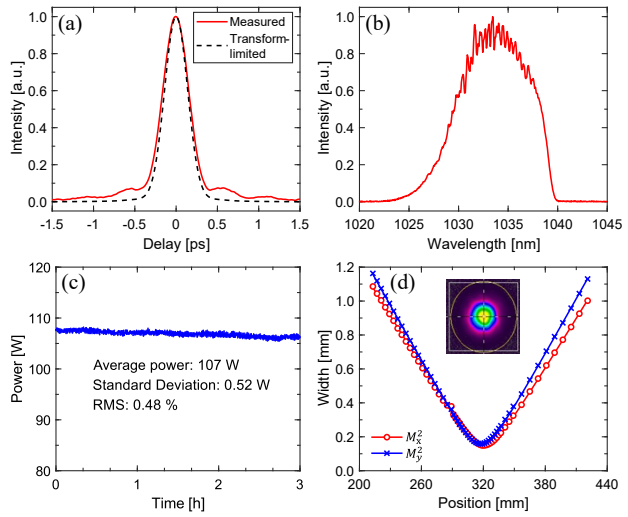

Fig. 6. (a) Measured autocorrelation (red) and transform-limited autocorrelation (black dashed) trace of the compressed pulse at 1.07 mJ energy. (b) Spectrum of the pulse. (c) Long-term power stability of the compressed pulse. (d) Horizontal (red) and vertical (blue) measured beam quality factor (M^2) of the compressed output beam.

pass through a pair of diffraction gratings configured in double-pass with an efficiency of 91%, which results in compressed pulses with 107 W average power and 1.07 mJ pulse energy. The black dashed curve in Fig. 6(a) represents the calculated autocorrelation trace of the transform-limited pulse corresponding the optical spectrum [Fig. 6(b)] of the compressed pulses. The transform-limited pulse duration is 237 fs. The red curve in Fig. 6(a) shows the measured autocorrelation trace with a full width at half-maximum (FWHM) of 370 fs. The pulse duration is estimated to be 240 fs assuming a pulse shape of hyperbolic-secant. The oscilloscope trace was measured in the nanosecond scale by a fast photodetector, and we did not observe noticeable satellite pulses. The rapid modulation appearing in the optical spectrum [Fig. 6(b)] is attributed to accumulated nonlinearities during the amplification [27].

We also analyzed the beam quality and long-term power stability of the compressed pulses. The long-term power stability of compressed output power at 107 W [Fig. 6(c)] is obtained by 3 h measurement and the root mean square (RMS) of average power is below 0.5% over 3 h, indicating excellent stability of passive CBC. A power decrease of 2.8 W occurs during 3 h, which can be mitigated by careful thermal management (e.g., better thermal isolation and active cooling of optical components). The M^2 measurement of the 1.07 mJ compressed pulses is depicted in Fig. 6(d), and near diffraction limited values of $M_x^2 = 1.11$ and $M_y^2 = 1.27$ are obtained. These values remain nearly the same at all energy levels. The inset of Fig. 6(d) shows the far-field beam profile, which has nearly Gaussian profile.

4. DISCUSSION AND CONCLUSION

In conclusion, we investigated the effect of SMD on average power limitation of passively combined Sagnac Yb-fiber amplifiers. We show that adding a polarization filter inside the Sagnac interferometer can mitigate SMD and increase both the combined average power and the combining efficiency. At 150 kHz repetition rate, our Sagnac Yb-fiber amplifier can deliver amplified pulses with up to 160 W average power; at 100 kHz repetition rate, the system generates 1.07 mJ, 240 fs pulses with 87% combining efficiency. Guichard *et al.* employed four spatiotemporal replicas together with a Sagnac interferometer to produce 300 fs pulses with 1.07 mJ energy and 55 W average power [23]. By mitigating the detrimental SMD effect, our results represent a factor of 2 improvement in terms of average power.

This femtosecond source with mJ-level pulse energy and hundred-watt average power is of particular importance for high-field science applications. Further energy scaling can be achieved by increasing the number of pulse replicas, which is limited by the nonlinear phase difference among pulse replicas as a result of gain saturation effect. This can be compensated by adjusting the energy distribution of these replicas prior to amplification. It is possible to generate 2 mJ pulses using four temporal replicas. Power scaling is limited by SMD rather than TMI. It seems that an increased TMI threshold also leads to a higher SMD threshold. Recently NKT reported generation of pulses with 248 W average power in a Yb-doped rod-type fiber of improved design for TMI suppression [28]. When these new rod-type fibers are incorporated into the Sagnac interferometer, generation of femtosecond pulses with mJ pulse energy and >300 W average power is possible.

Funding. National Key Research and Development Program of China (2021YFB3602602); National Natural Science Foundation of China (62175255, 62227822).

Disclosures. The method and apparatus reported here have been disclosed as intellectual property by J. S. W., G. Q. C., Y. Z., J. L. W., and Z. Y. W. to the Institute of Physics, Chinese Academy of Sciences, China.

Data availability. Data underlying the results presented in this paper are not publicly available at this time but may be obtained from the authors upon reasonable request.

REFERENCES

1. T. Eidam, J. Rothhardt, F. Stutzki, F. Jansen, S. Hädrich, H. Carstens, C. Jauregui, J. Limpert, and A. Tünnermann, "Fiber chirped-pulse amplification system emitting 3.8 GW peak power," Opt. Express **19**, 255–260 (2011).
2. P. Wan, L. M. Yang, and J. Liu, "All fiber-based Yb-doped high energy, high power femtosecond fiber lasers," Opt. Express **21**, 29854–29859 (2013).

3. H. Stark, M. Benner, J. Buldt, A. Klenke, and J. Limpert, "Pulses of 32 mJ and 158 fs at 20-kHz repetition rate from a spatiotemporally combined fiber laser system," Opt. Lett. **48**, 3007–3010 (2023).
4. M. Müller, C. Aleshire, A. Klenke, E. Haddad, F. Légaré, A. Tünnermann, and J. Limpert, "10.4 kW coherently combined ultrafast fiber laser," Opt. Lett. **45**, 3083–3084 (2020).
5. A. Klenke, M. Mueller, H. Stark, M. Kienel, C. Jauregui, A. Tünnermann, and J. Limpert, "Coherent beam combination of ultrafast fiber lasers," IEEE J. Sel. Top. Quantum Electron. **24**, 0902709 (2018).
6. L. Daniault, M. Hanna, D. N. Papadopoulos, Y. Zaouter, E. Mottay, F. Druon, and P. Georges, "Passive coherent beam combining of two femtosecond fiber chirped-pulse amplifiers," Opt. Lett. **36**, 4023–4025 (2011).
7. Y. Zaouter, L. Daniault, M. Hanna, D. N. Papadopoulos, F. Morin, C. Hönninger, F. Druon, E. Mottay, and P. Georges, "Passive coherent combination of two ultrafast rod type fiber chirped pulse amplifiers," Opt. Lett. **37**, 1460–1462 (2012).
8. L. Daniault, M. Hanna, D. N. Papadopoulos, Y. Zaouter, E. Mottay, F. Druon, and P. Georges, "High peak-power stretcher-free femtosecond fiber amplifier using passive spatio-temporal coherent combining," Opt. Express **20**, 21627–21634 (2012).
9. S. Zhou, F. W. Wise, and D. G. Ouzounov, "Divided-pulse amplification of ultrashort pulses," Opt. Lett. **32**, 871–873 (2007).
10. L. J. Kong, L. M. Zhao, S. Lefrancois, D. G. Ouzounov, C. X. Yang, and F. W. Wise, "Generation of megawatt peak power picosecond pulses from a divided-pulse fiber amplifier," Opt. Lett. **37**, 253–255 (2012).
11. Y. Zaouter, F. Guichard, L. Daniault, M. Hanna, F. Morin, C. Hönninger, E. Mottay, F. Druon, and P. Georges, "Femtosecond fiber chirped- and divided-pulse amplification system," Opt. Lett. **38**, 106–108 (2013).
12. F. Guichard, Y. Zaouter, M. Hanna, K. Mai, F. Morin, C. Hönninger, E. Mottay, F. Druon, and P. Georges, "Energy scaling of a nonlinear compression setup using passive coherent combining," Opt. Lett. **38**, 4437–4440 (2013).
13. J.-F. Lupi, M. M. Johansen, M. Michieletto, and J. Lægsgaard, "Static and dynamic mode coupling in a double-pass rod-type fiber amplifier," Opt. Lett. **43**, 5535–5538 (2018).
14. J. Lægsgaard, "Static thermo-optic instability in double-pass fiber amplifiers," Opt. Express **24**, 13429–13443 (2016).
15. T. Eidam, C. Wirth, C. Jauregui, F. Stutzki, F. Jansen, H.-J. Otto, O. Schmidt, T. Schreiber, J. Limpert, and A. Tünnermann, "Experimental observations of the threshold-like onset of mode instabilities in high power fiber amplifiers," Opt. Express **19**, 13218–13224 (2011).
16. H.-J. Otto, F. Stutzki, F. Jansen, T. Eidam, C. Jauregui, J. Limpert, and A. Tünnermann, "Temporal dynamics of mode instabilities in high-power fiber lasers and amplifiers," Opt. Express **20**, 15710–15722 (2012).
17. H.-J. Otto, N. Modsching, C. Jauregui, J. Limpert, and A. Tünnermann, "Impact of photodarkening on the mode instability threshold," Opt. Express **23**, 15265–15277 (2015).
18. C. Jauregui, C. Stihler, and J. Limpert, "Transverse mode instability," Adv. Opt. Photon. **12**, 429–484 (2020).
19. A. V. Smith and J. J. Smith, "Mode instability in high power fiber amplifiers," Opt. Express **19**, 10180–10192 (2011).
20. Y. Zhang, J. S. Wang, H. Teng, S. B. Fang, J. L. Wang, G. Q. Chang, and Z. Y. Wei, "Double-pass pre-chirp managed amplification with high gain and high average power," Opt. Lett. **46**, 3115–3118 (2021).
21. J.-F. Lupi, M. M. Johansen, M. Michieletto, S. L. Christensen, and J. Lægsgaard, "High gain in a dual-pass rod-type fiber amplifier," J. Opt. Soc. Am. B **37**, 451–458 (2020).
22. C. Stihler, H.-J. Otto, C. Jauregui, J. Limpert, and A. Tünnermann, "Experimental investigation of transverse mode instabilities in a double-pass Yb-doped rod-type fiber amplifier," Proc. SPIE **10083**, 100830R (2017).
23. F. Guichard, Y. Zaouter, M. Hanna, K. Mai, F. Morin, C. Hönninger, E. Mottay, and P. Georges, "High-energy chirped- and divided-pulse Sagnac femtosecond fiber amplifier," Opt. Lett. **40**, 89–92 (2015).
24. D. N. Schimpf, T. Eidam, E. Seise, S. Hädrich, J. Limpert, and A. Tünnermann, "Circular versus linear polarization in laser-amplifiers with Kerr-nonlinearity," Opt. Express **17**, 18774–18781 (2009).
25. S. Jiang, M. Hanna, F. Druon, and P. Georges, "Impact of self-phase modulation on coherently combined fiber chirped-pulse amplifiers," Opt. Lett. **35**, 1293–1295 (2010).
26. M. Kienel, A. Klenke, T. Eidam, M. Baumgartl, C. Jauregui, J. Limpert, and A. Tünnermann, "Analysis of passively combined divided-pulse amplification as an energy-scaling concept," Opt. Express **21**, 29031–29042 (2013).
27. A. Klenke, S. Hädrich, T. Eidam, J. Rothhardt, M. Kienel, S. Demmler, T. Gottschall, J. Limpert, and A. Tünnermann, "22 GW peak-power fiber chirped-pulse-amplification system," Opt. Lett. **39**, 6875–6878 (2014).
28. M. E. V. Pedersen, M. M. Johansen, A. S. Olesen, M. Michieletto, M. Gaponenko, and M. D. Maack, "175 W average power from a single-core rod fiber-based chirped-pulse-amplification system," Opt. Lett. **47**, 5172–5175 (2022).